Film conformality and extracted recombination probabilities of O atoms during plasma-assisted atomic layer deposition of SiO_2, TiO_2, $Al2O_3$, and HfO_2

THE JOURNAL OF PHYSICAL CHEMISTRY C

Article

Cite This: J. Phys. Chem. C 2019, 123, 27030−27035

pubs.acs.org/JPCC

Film Conformality and Extracted Recombination Probabilities of O Atoms during Plasma-Assisted Atomic Layer Deposition of SiO_2, TiO_2, Al_2O_3, and HfO_2

Karsten Arts,[†] Mikko Utriainen,[‡] Riikka L. Puurunen,[§,⊥] Wilhelmus M. M. Kessels,*[,†] and Harm C. M. Knoops*[,†,∥]

[†]Eindhoven University of Technology, P. O. Box 513, 5600 MB Eindhoven, The Netherlands

[‡]VTT Technical Research Centre of Finland, Tietotie 3, 02044 Espoo, Finland

[§]Aalto University School of Chemical Engineering, P. O. Box 16100, FI-00076 Aalto, Finland

[∥]Oxford Instruments Plasma Technology, North End, Bristol BS49 4AP, United Kingdom

Supporting Information

ABSTRACT: Surface recombination of plasma radicals is generally considered to limit film conformality during plasma-assisted atomic layer deposition (ALD). Here, we experimentally studied film penetration into high-aspect-ratio structures and demonstrated that it can give direct information on the recombination probability r of plasma radicals on the growth surface. This is shown for recombination of oxygen (O) atoms on SiO_2, TiO_2, Al_2O_3, and HfO_2 where a strong material dependence has been observed. Using extended plasma exposures, films of SiO_2 and TiO_2 penetrated extremely deep up to an aspect ratio (AR) of ∼900, and similar surface recombination probabilities of $r = (6 \pm 2) \times 10^{-5}$ and $(7 \pm 4) \times 10^{-5}$ were determined for these processes. Growth of Al_2O_3 and HfO_2 was conformal up to depths corresponding to ARs of ∼80 and ∼40, with r estimated at $(1-10) \times 10^{-3}$ and $(0.1-10) \times 10^{-2}$, respectively. Such quantitative insight into surface recombination, as provided by our method, is essential for modeling radical-surface interaction and understanding for which materials and conditions conformal film growth is feasible by plasma-assisted ALD.

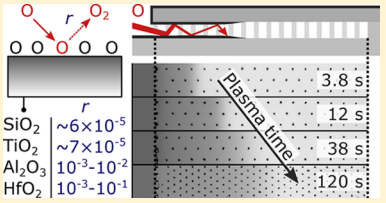

INTRODUCTION

Atomic layer deposition (ALD) is a well-established technique used for the synthesis of ultrathin conformal films with atomic-level thickness control.[1,2] This high level of conformality and thickness control is enabled by the self-limiting nature of the alternated precursor and coreactant steps. Plasma-assisted ALD, in which plasma is used as the coreactant, has further extended the capabilities of ALD, for instance, in terms of low-temperature processing and the number of materials deposited by ALD.[3,4] Examples of materials that have received notable interest are TiN and TaN as metal electrode and diffusion barriers, respectively,[5] SiO_2 and TiO_2 as spacer materials for self-aligned patterning,[6,7] and HfO_2 as a high-k dielectric.[8] In particular, the usage of SiO_2 in self-aligned multiple patterning has led to the breakthrough of plasma ALD in high-volume manufacturing.[4,6] For this application, plasma ALD enables the growth of SiO_2 at low temperature while providing the required high level of film conformality. Still, it is commonly believed that conformal film growth by plasma ALD is typically challenging due to the loss of reactive plasma radicals through surface recombination.

A theoretical understanding of the impact of surface recombination on film conformality during plasma ALD has been obtained in the literature, for instance, by Knoops et al.[9] and Dendooven et al.[10] using Monte Carlo simulations and by Yanguas-Gil and Elam[11] using a continuum model. In these models, a surface recombination probability r is used to describe the probability that a radical recombines upon collision with the growth surface where r typically ranges over several orders of magnitude from 10^{-5} up to 10^{-1}.[9] Importantly, it has been shown that r has a strong impact on the dose of plasma radicals needed to reach film saturation on high-aspect-ratio structures.[9,11] Moreover, it has been established that surface recombination often limits the aspect ratio (AR) up to which conformal film growth is practically achievable.[9,10,12] Still, quantitative information on r is barely reported in the literature and is typically only obtained by complex and indirect measurement techniques. However, such information is vital for modeling and predicting the film conformality obtained by plasma ALD processes.

In this article, we address this issue by determining surface recombination probabilities directly from the measured film conformalities. We theoretically show that the AR up to which film growth is achieved can be directly related to the value of r under typical process conditions. This is experimentally demonstrated for the recombination of oxygen radicals during

Received: August 27, 2019
Revised: October 15, 2019
Published: October 16, 2019

DOI: 10.1021/acs.jpcc.9b08176
J. Phys. Chem. C 2019, 123, 27030−27035

plasma ALD of SiO_2, TiO_2, Al_2O_3, and HfO_2 where we observe a strong material dependence.

MODELING

To derive the relation between the surface recombination probability and the penetration depth of a film grown by plasma ALD, we have adopted the continuum model reported by Yanguas-Gil and Elam (see the Supporting Information), which describes (plasma) ALD on one-dimensional high-AR structures with a constant diffusion coefficient D (m^2 s^{-1}).[11,13] In this reaction−diffusion model, the evolution of gas-phase reactant density $n(z, t)$ (m^{-3}) and surface coverage $\theta(z, t)$, defined as the reacted fraction of available reaction sites,[11,13,14] is described by the following dimensionless equations:

$$\frac{\partial \tilde{n}}{\partial \tau} - \frac{\partial^2 \tilde{n}}{\partial \xi^2} = -\eta s_0(1-\theta)\tilde{n} - \eta r \tilde{n} \quad (1)$$

$$\frac{\mathrm{d}\theta}{\mathrm{d}\tau} = \gamma \eta s_0(1-\theta)\tilde{n} \quad (2)$$

Here, the distance z (m) into the high-AR structure is normalized by the total structure length L (m) such that $\xi \equiv z/L$, the reactant exposure time t (s) is made dimensionless by $\tau \equiv tD/L^2$, and $\tilde{n} \equiv n/n_0$ represents the gas-phase reactant density normalized by the density n_0 (m^{-3}) at $z = 0$. Furthermore, η and γ are defined as $\eta \equiv \frac{1}{4}L^2\frac{S}{V}\frac{v_{th}}{D}$ and $\gamma \equiv \frac{Vn_0A_0}{S}$, where S/V is the surface to volume ratio of the structure (m^{-1}), v_{th} is the mean thermal velocity (m s^{-1}), and A_0 is the average effective area (m^2) of an adsorption site, which can be calculated from the growth per cycle (GPC).[11,15] The parameter η represents the ratio between the collision rate with the growth surface and the diffusion rate into the high-AR structure, while γ describes the number of reactant molecules simultaneously present in the structure per adsorption site. Aside from these mainly geometrical parameters, the evolution of n and θ is governed by the initial sticking probability s_0 (also referred to as initial reaction probability β_0)[11] and recombination probability r of the reactant upon collision with the growth surface. Note that here the surface chemistry is simplified by the adopted irreversible Langmuir model[11,13,14,16] and by assuming first-order recombination kinetics.[11] Accordingly, the term $-\eta s_0(1-\theta)\tilde{n}$ describes the loss of gas-phase reactant species through sticking reactions, providing film growth in a self-limiting way, while the term $-\eta r\tilde{n}$ describes the loss of reactive (co-)reactant species through surface recombination, which continues also after saturation of the surface coverage.

The impact of surface recombination on conformal plasma ALD is illustrated in Figure 1 where the shown radical density profiles and surface coverage outlines are computed using eqs 1 and 2. For these calculations, molecular flow (Knudsen approximation) in trenches with AR = 2000 and $\gamma \ll 1$ is assumed,[11,13] with an initial sticking probability of s_0=10^{-4}. The displayed results are representative for plasma ALD on the microscopic lateral high aspect ratio (LHAR) structures used in this work (PillarHall LHAR generation 3 and 4, developed by Puurunen and co-workers).[13,15,17−21] These trenches with extremely high AR values are formed by a polysilicon membrane, which is suspended above a c-Si substrate using a network of Si pillars. As a result, the LHAR trenches are oriented horizontally such that film growth by nondirectional

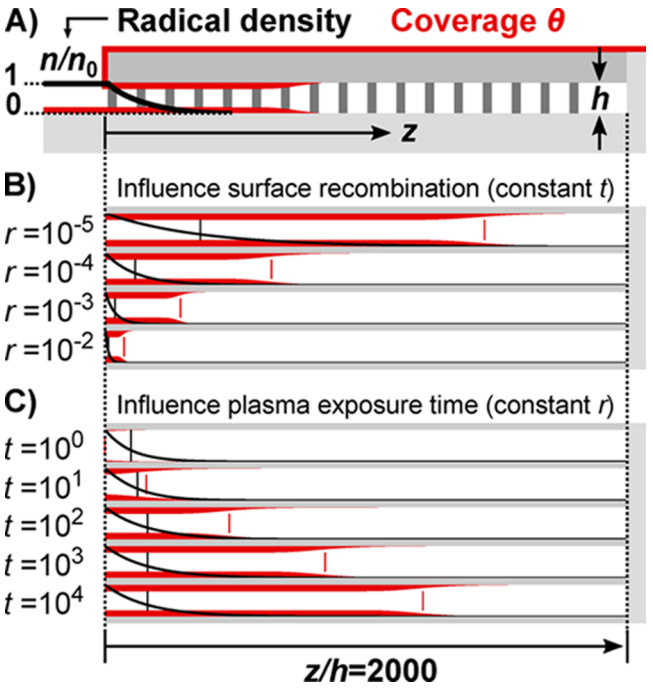

Figure 1. Panel (A) gives a schematic cross-sectional side view of a PillarHall LHAR structure used in this work to study film growth by plasma ALD. Through surface recombination, the density of plasma radicals decreases exponentially versus distance into the trench. This sets a practical limit on the penetration depth of the deposited film, as illustrated in panel (B) for different surface recombination probabilities and a constant time $t = 10^4$ (a.u.). For $r = 5 \times 10^{-5}$, panel (C) shows that an exponential increase in plasma exposure time is required to linearly increase the film penetration depth. The markers indicate the positions at which $\tilde{n} = 1/e$ and $\theta = 1/2$.

plasma radicals is obtained while excluding the directional ions. A schematic cross-sectional side view of a PillarHall LHAR structure is given in Figure 1a, also showing an illustrative radical density profile and film coverage. Figure 1b,c shows the actual simulation results for different values of r and plasma exposure time t (a.u.), respectively. As expected, the film penetration depth decreases with r and increases with t. More strikingly, Figure 1c shows that a steady-state exponential decrease in radical density is developed where the flux of incoming radicals is balanced by the recombination loss to the sidewalls. In this "recombination-limited" growth regime,[9] an exponential increase in t is required to linearly increase the film penetration depth.

While eqs 1 and 2 combined describe plasma ALD on a high-AR structure, only eq 1 is needed to predict the film penetration depth. This penetration depth is typically limited by the plasma half-cycle, for which n corresponds to the density of reactive plasma radicals. As discussed above, the plasma half-cycle is characterized by a recombination-limited growth regime where $\frac{\partial \tilde{n}}{\partial \tau} \approx 0$. Moreover, in this regime, $\frac{r}{s_0(1-\theta)} \gg 1$ such that the recombination loss $-\eta r\tilde{n}$ is much larger than the reaction loss $-\eta s_0(1-\theta)\tilde{n}$. Note that this is not only the case for a large r but also when film saturation is approached (i.e., $\theta \to 1$) in the region that needs to be passed by the radicals when diffusing to the growth front. The value of s_0 can therefore affect the shape of the coverage profile[11,13,14] but typically has a negligible effect on the penetration of

DOI: 10.1021/acs.jpcc.9b08176
J. Phys. Chem. C 2019, 123, 27030−27035

radicals into a high-AR structure during film growth. Under these conditions, eq 1 therefore reduces to

$$\frac{\partial^2 \tilde{n}}{\partial \xi^2} \approx \eta r \tilde{n} \tag{3}$$

Using the boundary conditions $\tilde{n}(0) = n(0)/n_0 = 1$ and $\lim_{\xi \to \infty} \tilde{n}(\xi) = 0$, eq 3 is solved to obtain a general expression for the recombination-limited radical density profile in a high-AR structure:

$$\tilde{n}(\xi) = \exp(-\sqrt{\eta r}\,\xi) \tag{4}$$

This exponential decrease in radical density is in line with Monte Carlo simulations reported by Knoops et al.[9] and can be used to obtain an expression for the 50% thickness penetration depth ($PD^{50\%}$)[22] as a function of the plasma exposure time t used in the ALD cycle. For this expression, we define the normalized penetration depth $\xi_{50\%} \equiv PD^{50\%}/L$ as the depth at which the dose of radicals needed for 50% saturation has been reached. Since the radical dose is proportional to $n(\xi)t$, we can state that $n(\xi_{50\%})t = n_0 t_{50\%}$, where $t_{50\%}$ is defined as the 50% saturation time at the entrance of the high-AR structure where $n(\xi) = n_0$. Using eq 4 for $n(\xi_{50\%})$, this gives $\exp(-\sqrt{\eta r}\,\xi_{50\%})t = t_{50\%}$, which is rewritten as

$$\xi_{50\%}(t) = \frac{1}{\sqrt{\eta r}} \ln\left(\frac{t}{t_{50\%}}\right) \tag{5}$$

As already seen in Figure 1c, eq 5 shows that the film penetration depth increases logarithmically with t, where the magnitude of this increase is determined by η and r. For a high-AR structure with a known η, eq 5 can thus be used to determine r.

In this work, we determine r using the PillarHall LHAR trenches described in Figure 1a. For a typical process pressure (50 mtorr in this work), the nominal gap height of h = 500 nm is low enough to assume molecular flow, as the mean free path λ_{mfp} ~0.1 mm $\gg h$.[22] In this case, $D = \frac{2}{3} v_{th} h$ such that $\eta = \frac{1}{4} L^2 \frac{S}{V} \frac{v_{th}}{D}$ is independent of v_{th}.[13,15] Together with $\frac{S}{V} = \frac{2}{h}$, this gives $\eta = \frac{3}{4}\left(\frac{L}{h}\right)^2$ for molecular flow in a trench. Using this expression for η, eq 5 can be written as

$$\tilde{z}_{50\%}(t) = \frac{1}{\sqrt{\frac{3}{4} r}} \ln\left(\frac{t}{t_{50\%}}\right) \tag{6}$$

where $\tilde{z}_{50\%} \equiv \frac{PD^{50\%}}{h} = \xi_{50\%} \frac{L}{h}$ is the aspect ratio at 50% thickness penetration depth. Without information on $t_{50\%}$, measuring and plotting $\tilde{z}_{50\%}$ as a function of $\ln(t)$ directly provide the value of r, as the slope is equal to $1/\sqrt{\frac{3}{4} r}$. This method will be demonstrated in Figure 3. Note that a different value of $t_{50\%}$ shifts the $\tilde{z}_{50\%}$ data but does not affect the slope and determined value of r. If only one value of $\tilde{z}_{50\%}$ is known, a rough value of r can be calculated using eq 6 by estimating $t_{50\%}$ from the saturation time of the plasma half-cycle. Both approaches are used here to determine the recombination probabilities of O atoms during plasma ALD of SiO_2, TiO_2, Al_2O_3, and HfO_2, under the assumption that film growth by species other than the supplied O radicals can be neglected for these processes.

EXPERIMENTAL DETAILS

The depositions were carried out in a commercial ALD system (Oxford Instruments FlexAL) where O_2/Ar plasma was generated by a remote inductively coupled plasma source operated at 13.56 MHz.[23] The precursors used were $SiH_2(N(C_2H_5)_2)_2$ (BDEAS), $Ti(N(CH_3)_2)_4$ (TDMAT), $Al(CH_3)_3$ (TMA), and $HfCp(N(CH_3)_2)_3$ (TDMACpH) for the growth of SiO_2, TiO_2, Al_2O_3, and HfO_2, respectively. In all recipes, a sufficiently high precursor dose was used such that the plasma half-cycles were limiting the film penetration.[13] To properly compare the different plasma ALD processes, the plasma conditions were kept constant (i.e., 100/50 sccm O_2/Ar gas mixture, 50 mtorr pressure, and 600 W ICP power) and all depositions were carried out at a table temperature set-point of 200 °C. Plasma exposure times ranging from 3.8 up to 120 s were used where it is noted that the shorter plasmas have a relatively higher uncertainty due to striking time and other startup effects.

After deposition, the polysilicon membrane of each PillarHall LHAR structure[13,15,17−21] was removed using adhesive tape such that the deposited film and its penetration depth could be analyzed using top-view diagnostics. Figure 2a shows optical microscope images of the structures after deposition and removal of the membrane. Due to thin-film interference, the darker regions correspond to surface area with a deposited film. These regions start at the top, where the cavity entrance was located, and extend downward to a certain penetration depth into the cavity. Different PillarHall versions were used where based on previous results the trench version should not affect the thickness profile of the deposited film. The versions used are as follows (from left to right in Figure 2): LHAR4-ADVANCED trench W90 L1020 (3.8, 12, and 38 s SiO_2), LHAR3-v1a trench W100L5mm (120 s SiO_2), LHAR4 small chip vS2 (12 s TiO_2) and vS1 (120 s TiO_2), LHAR4-ADVANCED trench W90 L1020 (120 s Al_2O_3), and LHAR4 small chip vS2 (120 s HfO_2).

The 50% thickness penetration depths indicated in Figure 2a were determined in Figure 2b from the thickness profiles of the deposited films, which were measured by a Filmetrics F40-UV. This reflectometer has a spot size of ~10 μm and was used in combination with a motorized mapping stage (Filmetrics StageBase-XY10-Auto-100 mm) to resolve the thickness profiles with a spatial resolution of 5 μm. The displayed data was normalized by the thickness obtained just inside the cavity, which approximately corresponded to 60 nm SiO_2 (400 cycles), 26 nm TiO_2 (400 cycles), 39 nm Al_2O_3 (300 cycles), and 37 nm HfO_2 (300 cycles).

RESULTS AND DISCUSSION

The measurements shown in Figure 2 demonstrate that penetration up to extremely high AR values is obtained for SiO_2 and TiO_2, approaching AR ~900 when using 120 s plasma half-cycles. The increase in $PD^{50\%}$ with plasma time confirms that film penetration was limited by the plasma half-cycle. This was also verified for the Al_2O_3 and HfO_2 processes where film penetration at t = 120 s reached ARs of ~80 and ~40, respectively, suggesting a significantly larger effect of surface recombination. The relatively low conformality of Al_2O_3 and HfO_2 compared with SiO_2 and TiO_2 is in line with

DOI: 10.1021/acs.jpcc.9b08176
J. Phys. Chem. C 2019, 123, 27030−27035

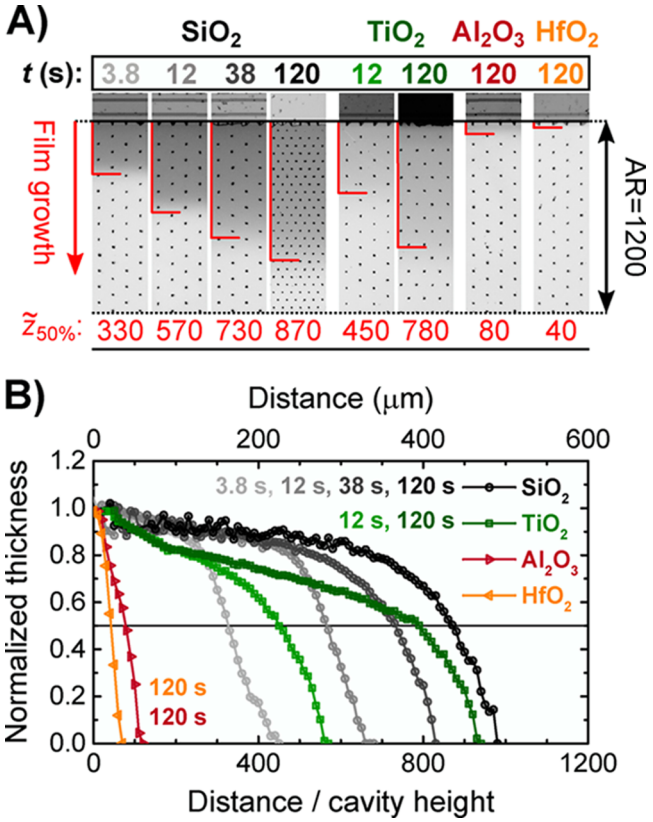

Figure 2. (A) Top view optical microscope images of PillarHall LHAR structures, after plasma ALD of SiO_2, TiO_2, Al_2O_3, or HfO_2 and removal of the membrane (note that PillarHall generation 3, which has a smaller pillar spacing than PillarHall-4, was used for SiO_2 growth using 120 s plasma steps). Surface areas with deposited material are darker by thin-film interference. These areas start at the cavity entrance (top) and extend downward to a certain penetration depth. The aspect ratios at $PD^{50\%}$ are indicated in red, as determined in panel (B) from the measured thickness profiles. A strong variation in film penetration depth is observed, revealing that the surface recombination of plasma radicals is highly material-dependent.

results reported in the literature, obtained using similar plasma ALD conditions as in this work.[24−26] For example, Dingemans et al. obtained >95% conformality for SiO_2 opposed to ∼50% conformality for Al_2O_3 on a trench with an AR of ∼30.[24] Similar to this result for SiO_2, Schindler et al. achieved a step coverage of >90% for TiO_2 deposited on trench-like holes with AR = 30.[25] In contrast, the conformality of HfO_2, as reported by Sharma et al., was limited to ∼70% on a trench with AR = 7.3.[26] Nevertheless, using a different precursor, Kariniemi et al. reported conformal plasma ALD of HfO_2 on trenches with AR = 60,[27] indicating that a higher conformality may be obtained under different experimental conditions.

The large difference in film penetration between SiO_2 and TiO_2 on the one hand and Al_2O_3 and HfO_2 on the other hand indicates that the surface recombination and film conformality during plasma ALD are heavily material-dependent. For SiO_2 and TiO_2, the surface recombination probability appears to be low enough to meet conformality requirements in very demanding applications, while the Al_2O_3 and HfO_2 processes should be able to provide conformal film growth on structures with AR values of 10 to 30 within acceptable cycle times.

In Figure 3, the film penetration $\tilde{z}_{50\%} \equiv PD^{50\%}/h$ for SiO_2 and TiO_2 is plotted against the natural logarithm of the plasma

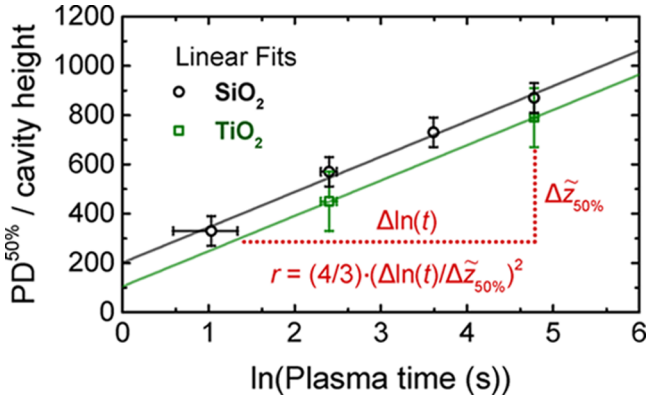

Figure 3. Film penetration for plasma ALD of SiO_2 and TiO_2, as presented in Figure 2, plotted against the natural logarithm of the plasma exposure time. Here, a one second uncertainty in plasma time has been included to account for variation in striking time and other startup effects. The slope of this plot provides the effective surface recombination probability of radicals during the plasma ALD process. For the SiO_2 and TiO_2 processes, very similar values of $r = (6 \pm 2) \times 10^{-5}$ and $(7 \pm 4) \times 10^{-5}$ are determined.

exposure time used in the ALD cycle, showing a linear relation as expected from eq 6. For these two processes, a very similar slope is found, corresponding to a fitted surface recombination probability of $(6 \pm 2) \times 10^{-5}$ for SiO_2 and $(7 \pm 4) \times 10^{-5}$ for TiO_2. For the Al_2O_3 and HfO_2 processes, r is estimated to be in the ranges of $(1-10) \times 10^{-3}$ and $(0.1-10) \times 10^{-2}$, respectively. These rough values of r for Al_2O_3 and HfO_2 have been calculated directly using eq 6, where $t_{50\%}$ is estimated to lie between 0.2 and 2 s for the Al_2O_3 process and between 0.2 and 8 s for the HfO_2 process, based on saturation curves reported by Dingemans et al.[24] and Sharma et al.[26] For the SiO_2 and TiO_2 processes, $t_{50\%}$ follows directly from the linear fits shown in Figure 3, giving 0.25 ± 0.07 and (0.1−2) s, respectively.

The results are summarized in Table 1, indicating a good agreement with the literature data available. Note that for TiO_2

Table 1. Recombination Probabilities r of O Radicals on Different Material Surfaces, As Determined in This Work and As Reported in the Literature

material	determined r	literature value r
SiO_2	$(6 \pm 2) \times 10^{-5}$	$(2 \pm 1) \times 10^{-4}$,[a] 1.6×10^{-4},[b] $(3-5) \times 10^{-5}$,[c] $(4-160) \times 10^{-4}$,[d] $(0.8-3) \times 10^{-5}$[e]
TiO_2	$(7 \pm 4) \times 10^{-5}$	
Al_2O_3	$(1-10) \times 10^{-3}$	2.1×10^{-3}[f]
HfO_2	$(0.1-10) \times 10^{-2}$	

[a]Ref 28. [b]Ref 32. [c]Ref 32 (Pyrex,[33] ∼81% SiO_2). [d]Ref 29 (Pyrex). [e]Ref 34 (Vycor,[35] ∼96% SiO_2). [f]Ref 32.

and HfO_2 no literature values have been found and that the values reported for O atom recombination on SiO_2 or SiO_2-based surfaces (i.e., Pyrex or Vycor glass) show a large spread. Aside from the measurement accuracy, several experimental factors such as temperature[28−30] and pressure[31] can cause this spread. Moreover, the surface treatment[29,32] and roughness[28] can play an important role. This is where our method shows merit in terms of relevance, as it provides the recombination probability on the actual growth surface during plasma ALD. Note that the properties of the saturated surface during plasma

DOI: 10.1021/acs.jpcc.9b08176
J. Phys. Chem. C 2019, 123, 27030−27035

exposure could depend on the precursor used (e.g., by residual hydrogen and carbon content), which may also influence the recombination probability.

An important open question that has received limited attention in the literature is the fundamental reason behind the material dependence of r. From an atomistic modeling perspective, key factors that play a role are, for instance, the amount of recombination sites and the activation energies for recombination and surface diffusion.[28,29] Moreover, r could be related to measurable material properties such as surface acidity.[32] By determining values of r for different materials and experimental conditions, our method can help in gaining essential insight into the fundamental mechanisms behind surface recombination.

CONCLUSIONS

In conclusion, we have established a powerful and straightforward method to study film conformality during plasma ALD and quantify the recombination probability r of plasma radicals on the growth surface. It was shown that the film penetration depth into high-AR structures is generally limited by surface recombination, in which case an exponential increase in plasma exposure time is required to linearly increase the film penetration. This relation gives direct quantitative information on r, as demonstrated for surface recombination of oxygen radicals during plasma ALD of SiO_2, TiO_2, Al_2O_3, and HfO_2. Low values of r on the order of 10^{-5} were determined for SiO_2 and TiO_2, corresponding to extremely deep film penetration approaching an AR of ∼900 at long plasma exposures. In contrast, plasma ALD of Al_2O_3 and HfO_2 was limited to ARs of ∼80 and ∼40, respectively, with r lying in the range of 10^{-3} up to 10^{-1}. This shows a strong material dependence in the surface recombination of plasma radicals and film conformality during plasma ALD. For the investigated processes, especially for SiO_2 and TiO_2, r seems sufficiently low to meet very demanding conformality requirements. We thus provide valuable insights for gaining quantitative knowledge on surface recombination of radicals and the film conformality achievable by plasma ALD.

ASSOCIATED CONTENT

Supporting Information

The Supporting Information is available free of charge on the ACS Publications website at DOI: 10.1021/acs.jpcc.9b08176.

Further details on the employed mathematical model and the derivation of the reported equations, based on the earlier work of Yanguas-Gil and Elam (ref 11) (PDF)

AUTHOR INFORMATION

Corresponding Authors

*E-mail: w.m.m.kessels@tue.nl (W.M.M.K.).
*E-mail: h.c.m.knoops@tue.nl (H.C.M.K.).

ORCID

Karsten Arts: 0000-0003-4266-6559
Wilhelmus M. M. Kessels: 0000-0002-7630-8226
Harm C. M. Knoops: 0000-0003-2284-4477

Notes

The authors declare the following competing financial interest(s): RLP has developed the microscopic PillarHall LHAR conformality test concept and is inventor of a related patent application. VTT has made PillarHall test structure prototypes available for purchase. MU is responsible for PillarHall test structure sales and commercialization activities at VTT.

⊥Present address: VTT Technical Research Centre of Finland, Tietotie 3, 02044 Espoo, Finland (R.L.P.).

ACKNOWLEDGMENTS

This work is part of the research program HTSM with Project No. 15352, which is (partly) financed by the Netherlands Organization for Scientific Research (NWO). PillarHall LHAR fabrication was carried out in the OtaNano research infrastructure. VTT acknowledges the financial support for developing the LHAR4 conformality test structure from Business Finland (National Innovation Funding Center of Finland, previously Tekes) through the PillarHall TUTL project.

REFERENCES

(1) George, S. M. Atomic Layer Deposition: An Overview. *Chem. Rev.* **2010**, *110*, 111−131.
(2) Puurunen, R. L. Surface Chemistry of Atomic Layer Deposition: A Case Study for the Trimethylaluminum/Water Process. *J. Appl. Phys.* **2005**, *97*, 121301.
(3) Profijt, H. B.; Potts, S. E.; van de Sanden, M. C. M.; Kessels, W. M. M. Plasma-Assisted Atomic Layer Deposition: Basics, Opportunities, and Challenges. *J. Vac. Sci. Technol., A* **2011**, *29*, No. 050801.
(4) Knoops, H. C. M.; Faraz, T.; Arts, K.; Kessels, W. M. M. Status and Prospects of Plasma-Assisted Atomic Layer Deposition. *J. Vac. Sci. Technol., A* **2019**, *37*, No. 030902.
(5) Kim, H. Atomic Layer Deposition of Metal and Nitride Thin Films: Current Research Efforts and Applications for Semiconductor Device Processing. *J. Vac. Sci. Technol., B: Microelectron. Nanometer Struct. –Process., Meas., Phenom.* **2003**, *21*, 2231.
(6) Beynet, J.; Wong, P.; Miller, A.; Locorotondo, S.; Vangoidsenhoven, D.; Yoon, T.-H.; Demand, M.; Park, H.-S.; Vandeweyer, T.; Sprey, H.; et al. Low Temperature Plasma-Enhanced ALD Enables Cost-Effective Spacer Defined Double Patterning (SDDP). *Proc. SPIE* **2009**, *7520*, 75201J.
(7) Raley, A.; Thibaut, S.; Mohanty, N.; Subhadeep, K.; Nakamura, S.; Ko, A.; O'Meara, D.; Tapily, K.; Consiglio, S.; Biolsi, P. Self-Aligned Quadruple Patterning Integration Using Spacer on Spacer Sub-32nm Pitch Applications. *Proc. SPIE* **2016**, *9782*, 97820F.
(8) Choi, J. H.; Mao, Y.; Chang, J. P. Development of Hafnium Based High- k Materials - A Review. *Mater. Sci. Eng. R* **2011**, *72*, 97−136.
(9) Knoops, H. C. M.; Langereis, E.; van de Sanden, M. C. M.; Kessels, W. M. M. Conformality of Plasma-Assisted ALD: Physical Processes and Modeling. *J. Electrochem. Soc.* **2010**, *157*, G241−G249.
(10) Dendooven, J.; Deduytsche, D.; Musschoot, J.; Vanmeirhaeghe, R. L.; Detavernier, C. Conformality of Al_2O_3 and AlN Deposited by Plasma-Enhanced Atomic Layer Deposition. *J. Electrochem. Soc.* **2010**, *157*, G111−G116.
(11) Yanguas-Gil, A.; Elam, J. W. Self-Limited Reaction-Diffusion in Nanostructured Substrates: Surface Coverage Dynamics and Analytic Approximations to ALD Saturation Times. *Chem. Vap. Deposition* **2012**, *18*, 46−52.
(12) Knoops, H. C. M.; Elam, J. W.; Libera, J. A.; Kessels, W. M. M. Surface Loss in Ozone-Based Atomic Layer Deposition Processes. *Chem. Mater.* **2011**, *23*, 2381−2387.
(13) Arts, K.; Vandalon, V.; Puurunen, R. L.; Utriainen, M.; Gao, F.; Kessels, W. M. M.; Knoops, H. C. M. Sticking Probabilities of H_2O and $Al(CH_3)_3$ during Atomic Layer Deposition of Al_2O_3 Extracted from Their Impact on Film Conformality. *J. Vac. Sci. Technol., A* **2019**, *37*, No. 030908.
(14) Dendooven, J.; Deduytsche, D.; Musschoot, J.; Vanmeirhaeghe, R. L.; Detavernier, C. Modeling the Conformality of Atomic Layer

DOI: 10.1021/acs.jpcc.9b08176
J. Phys. Chem. C 2019, 123, 27030−27035

Deposition: The Effect of Sticking Probability. *J. Electrochem. Soc.* **2009**, *156*, P63.
(15) Ylilammi, M.; Ylivaara, O. M. E.; Puurunen, R. L. Modeling Growth Kinetics of Thin Films Made by Atomic Layer Deposition in Lateral High-Aspect-Ratio Structures. *J. Appl. Phys.* **2018**, *123*, 205301.
(16) Masel, R. I. *Principle of Adsorption and Reaction on Solid Surfaces*; John Wiley & Sons: New York, 1996.
(17) Gao, F.; Arpiainen, S.; Puurunen, R. L. Microscopic Silicon-Based Lateral High-Aspect-Ratio Structures for Thin Film Conformality Analysis. *J. Vac. Sci. Technol., A* **2015**, *33*, No. 010601.
(18) Mattinen, M.; Hämäläinen, J.; Gao, F.; Jalkanen, P.; Mizohata, K.; Räisänen, J.; Puurunen, R. L.; Ritala, M.; Leskelä, M. Nucleation and Conformality of Iridium and Iridium Oxide Thin Films Grown by Atomic Layer Deposition. *Langmuir* **2016**, *32*, 10559−10569.
(19) Puurunen, R. L.; Gao, F. Influence of ALD Temperature on Thin Film Conformality: Investigation with Microscopic Lateral High-Aspect-Ratio Structures. In *2016 14th International Baltic Conference on Atomic Layer Deposition (BALD)*; IEEE, 2016, DOI: 10.1109/BALD.2016.7886526.
(20) Kia, A. M.; Haufe, N.; Esmaeili, S.; Mart, C.; Utriainen, M.; Puurunen, R. L.; Weinreich, W. ToF-SIMS 3D Analysis of Thin Films Deposited in High Aspect Ratio Structures via Atomic Layer Deposition and Chemical Vapor Deposition. *Nanomaterials* **2019**, *9*, 1035.
(21) Souqui, L.; Högberg, H.; Pedersen, H. Surface-Inhibiting Effect in Chemical Vapor Deposition of Boron−Carbon Thin Films from Trimethylboron. *Chem. Mater.* **2019**, *31*, 5408−5412.
(22) Cremers, V.; Puurunen, R. L.; Dendooven, J. Conformality in Atomic Layer Deposition: Current Status Overview of Analysis and Modelling. *Appl. Phys. Rev.* **2019**, *6*, No. 021302.
(23) Heil, S. B. S.; van Hemmen, J. L.; Hodson, C. J.; Singh, N.; Klootwijk, J. H.; Roozeboom, F.; van de Sanden, M. C. M.; Kessels, W. M. M. Deposition of TiN and HfO_2 in a Commercial 200 Mm Remote Plasma Atomic Layer Deposition Reactor. *J. Vac. Sci. Technol., A* **2007**, *25*, 1357.
(24) Dingemans, G.; van Helvoirt, C. A. A.; Pierreux, D.; Keuning, W.; Kessels, W. M. M. Plasma-Assisted ALD for the Conformal Deposition of SiO_2: Process, Material and Electronic Properties. *J. Electrochem. Soc.* **2012**, *159*, H277−H285.
(25) Schindler, P.; Logar, M.; Provine, J.; Prinz, F. B. Enhanced Step Coverage of TiO_2 Deposited on High Aspect Ratio Surfaces by Plasma-Enhanced Atomic Layer Deposition. *Langmuir* **2015**, *31*, 5057−5062.
(26) Sharma, A.; Longo, V.; Verheijen, M. A.; Bol, A. A.; Kessels, W. M. M. Atomic Layer Deposition of HfO_2 Using $HfCp(NMe_2)_3$ and O_2 Plasma. *J. Vac. Sci. Technol., A* **2017**, *35*, No. 01B130.
(27) Kariniemi, M.; Niinistö, J.; Vehkamäki, M.; Kemell, M.; Ritala, M.; Leskelä, M.; Putkonen, M. Conformality of Remote Plasma-Enhanced Atomic Layer Deposition Processes: An Experimental Study. *J. Vac. Sci. Technol., A* **2012**, *30*, No. 01A115.
(28) Kim, Y. C.; Boudart, M. Recombination of oxygen, nitrogen, and hydrogen Atoms on Silica: Kinetics and Mechanism. *Langmuir* **1991**, *7*, 2999−3005.
(29) Macko, P.; Veis, P.; Cernogora, G. Study of Oxygen Atom Recombination on a Pyrex Surface at Different Wall Temperatures by Means of Time-Resolved Actinometry in a Double Pulse Discharge Technique. *Plasma Sources Sci. Technol.* **2004**, *13*, 251−262.
(30) Greaves, J. C.; Linnett, J. W. Recombination of Atoms at Surfaces. Part 6 - Recombination of Oxygen Atoms on Silica From 20°C to 600°C. *Trans. Faraday Soc.* **1959**, *55*, 1355−1361.
(31) Lopaev, D. V.; Malykhin, E. M.; Zyryanov, S. M. Surface Recombination of Oxygen Atoms in O_2 Plasma at Increased Pressure: I. the Recombination Probability and Phenomenological Model of Surface Processes. *J. Phys. D: Appl. Phys.* **2011**, *44*, No. 015201.
(32) Greaves, J. C.; Linnett, J. W. Recombination of Atoms at Surfaces. Part 5 - Oxygen Atoms at Oxide Surfaces. *Trans. Faraday Soc.* **1959**, *55*, 1346−1354.
(33) National Institute of Standards and Technology. *Composition of Pyrex Glass*. https://physics.nist.gov/cgi-bin/Star/compos.pl?matno=169, 2019.
(34) Berkowitz-Mattuck, J. B. *The Structure and Chemistry of Solid Surfaces*; Somorjai, G. A., Ed.; John Wiley & Sons: New York, 1969.
(35) Präzisions Glas; Optik GmbH. *Vycor 7913*. https://www.pgo-online.com/intl/vycor.html. 2019.

DOI: 10.1021/acs.jpcc.9b08176
J. Phys. Chem. C 2019, 123, 27030−27035